Optically transparent ceramics by spark plasma sintering of oxide nanoparticles

Rachman Chaim,[a,*] Rachel Marder[a] and Claude Estournès[b]

[a]*Department of Materials Engineering, Technion – Israel Institute of Technology, Haifa 32000, Israel*
[b]*CNRS, Institut Carnot Cirimat, F-31602 Toulouse Cedex 9, France*

Optical transparency in polycrystalline ceramic oxides can be achieved if the material is fully densified. Spark plasma sintering (SPS) of oxide nanoparticles leads to immediate densification with final-stage sintering. Further densification by annihilation of the isolated pores is associated with diffusional processes, regardless of the densification mechanism during the intermediate stage. Densification equations in conjunction with the concept of grain boundary free volume were used to derive the pore size–grain size–temperature map for designing the nanopowder and SPS process parameters to obtain transparent oxides.

Keywords: Sintering; Nanocrystalline materials; Optical transmission; Theory

Recently, appreciable attention has been paid to the investigation and fabrication of high melting point, optically transparent polycrystalline ceramic oxides. Optically transparent ceramics are often fabricated by either hot-isostatic pressing (HIP), or vacuum sintering at very high temperatures using ultrapure ultrafine powders [1–6]. Combining the high sinterability of nanocrystalline (nc) powders with the rapid densification rates characteristic of spark plasma sintering (SPS), the latter technique has been widely promoted as a method for fabricating transparent polycrystalline oxides [7–19]: transparent polycrystalline ceramics of various technical oxides, such as Al_2O_3 [7–11], MgO [12], $MgAl_2O_4$ spinel [12–17], mullite ($3Al_2O_3{\cdot}2SiO_2$) [18], YAG ($Y_3Al_5O_{12}$) [19], Y_2O_3 [20] and yttria-stabilized ZrO_2 [21,22] have been fabricated by SPS. However, these polycrystalline oxides, with either nanometric or micrometric grains, did not exhibit the expected theoretical inline transmittance (~85%), especially at the ultraviolet and the low visible wavelengths. This optical behavior may be explained by the presence of pores that are often observed at the grain junctions of ceramics subjected to SPS [7,8,13,19,21]. These residual pores are in the same size range as the incident wavelengths, and act as efficient scattering sources at a corresponding wavelength [23–25]. As was noted in a recent review on transparent ceramics, 100 ppm of porosity may reduce the intensity of the transmitted light by 50–70%, with an increase in the ceramic refraction index [25]. Consequently, this low volume fraction of pores should be eliminated when highly transparent polycrystalline ceramics in the visible range are desired. The present paper describes the densification behavior of oxide nanoparticles during SPS towards fully dense structures. Well-developed sintering theories were used to assess the SPS conditions at which fully dense transparent polycrystalline oxides may be formed.

Rapid densification during the heating-up stage to final-stage sintering is the main characteristic of SPS observed in nanopowder compacts under constant applied pressure. The rapid shrinkage during the second-stage sintering may proceed via two different processes. First, the nanoparticles can yield plastically at their contact points, provided that the effective applied stress at these points reaches the yield stress at the corresponding SPS temperature. Therefore, simultaneous application of high pressures and elevated temperature may lead to highly dense compacts, the structure of which is comparable to that at the end of second-stage sintering. The resulting nano-/microstructure consist of isolated nano-/micropores located at the grain junctions [26]. In this respect, the dependence of the yield stress on temperature and particle size, especially for nanoparticle aggregates, and the strain-hardening coefficient, will

* Corresponding author. Tel.: + 972-4-8294589; fax: +972-4-8295677; e-mail: rchaim@technion.ac.il

doi:10.1016/j.scriptamat.2010.03.056

affect the final dense microstructure. As the isolated pore size decreases into the nanometer range, its internal pressure may increase above the applied pressure if it contains an insoluble gas; hence, pore closure may cease [27]. Further densification by nanopore annihilation may proceed only by time-dependent diffusional processes.

Second, when the effective applied pressure is not sufficient to attain the yield stress, diffusional processes may become active. Densification may proceed by sliding of the nanoparticles over each other, preferably by surface and grain boundary (GB) diffusion. However, there are increasing numbers of experimental observations which confirm that sliding in both granular systems and dense nc materials proceeds in a cooperative manner [28–30]. This is believed to arise from the minimization of the energy needed to slide a high volume fraction of the interfaces, especially in the nc materials. Consequently, densification of non-close-packed nanoparticle aggregate by particles sliding over each other follows the same physical rules. The probability that a single nanoparticle will slide decreases as the densification proceeds. Once denser regions are formed, further densification will be followed by cooperative sliding of these regions over each other. The densification process via sliding will experience increasing resistance with the accumulated strain, due to the growth of dense nanoparticle clusters. The resultant microstructure may consist of dense clusters of nanograins, often separated by low-angle grain boundaries; larger nanograin clusters may be separated by high-angle grain boundaries, similar to that reported for nc-YAG [31]. Again, the evolved nano-/microstructure consists of isolated pores [4,8,32] which may be annihilated only by long-term diffusion, as mentioned above.

Therefore, regardless of the second-stage sintering mechanism, densification at the isothermal SPS temperature is associated with the final stage of sintering, when only isolated pores are present. Full densification for maximum transparency thus necessitates the elimination of these closed pores for extended SPS durations. In this respect, several materials and SPS process parameters can be controlled, and through them full densification to optical transparency may be achieved. Control of the SPS temperature in conjunction with the average grain and pore size at the final stage of sintering will be considered below.

In order to reach full theoretical density during SPS, further densification is associated with simultaneous grain growth. This, in turn, will reduce the total area of the GBs with typically lower density than a crystal density. The grain growth rate may be controlled either by the GB mobility or the pore mobility. When the mobility of the GB is higher than that of the nanopores (grain-size normalized mobility), one may expect detachment of the GB from the pore and resultant residual pores within the growing grains. Further annihilation of pores within the grain necessitates lattice diffusion that in practice cannot be achieved at low SPS temperatures. Rapid annihilation of the isolated nanopores by GB diffusion may be possible as long as these nanopores are attached to the GBs.

As long as the pore mobility is lower than the GB mobility, the latter is pinned by the nanopores which control the grain growth kinetics. This may provide conditions for grain growth stagnation, while densification proceeds as modeled, and as has been observed in several systems [33–35]. For the limiting case, when the two mobilities are equal, the pore is attached to the moving GB and may be annihilated by vacancy diffusion along the GB. Following Brook's [35] approach, the driving forces and the mobilities of the pores and the GBs were compared, and the conditions for densification were derived [27,36–38]. Similar analysis for tetrahedral (Reuleaux) nanopores located at all corners of tetrakaidecahedral (TKDH) nanograins was performed. The pore shrinkage rate for this model at constant grain size is [32]:

$$\left(\frac{dr}{dt}\right)_G = \frac{24(\sqrt{2}-1)\Omega}{(\pi-\sqrt{3})r^2}\frac{D_{gb}\delta_{gb}}{kT}\left(\frac{\gamma_{sv}}{r}+\frac{P_a}{\rho}\right), \tag{1}$$

where the pore coarsening rate at constant density is given by [32,37]:

$$\left(\frac{dr}{dt}\right)_\rho = \frac{1.2\Omega\cdot\gamma_{gb}}{28.6}\frac{D_s\delta_s}{kT}\frac{G}{r^4}(17.9-6.2\phi). \tag{2}$$

Here D_{gb} and D_s are the diffusion coefficients of the slowest ionic specie along the GB, and at the pore surface, respectively; δ_{GB} is the GB width, and δ_s is the depth at which surface diffusion is effective; r is the pore radius, G is the grain diameter, P_a is the applied pressure, γ_{sv} and γ_{GB} are the solid–gas surface energy and grain boundary energy, respectively; ρ is the original density (i.e. 0.925 at the final-stage sintering), ϕ is the tetrahedron apex angle, T is the temperature and k is the Boltzmann constant.

For a nanopore to shrink steadily, it should be attached to the GB, i.e. the pore shrinkage rate should be higher than the pore coarsening rate. This leads to the first condition as given by [32]:

$$168\frac{D_{gb}\delta_{gb}}{D_s\delta_s}r^2\left(\frac{\gamma_{sv}}{r}+\frac{P_a}{\rho}\right) > G(17.9-6.2\phi). \tag{3}$$

This relation was previously used to determine the grain size–pore size–temperature map at which densification may proceed with minimal grain growth.

However, full densification with the fastest kinetics may involve grain growth as long as pores are located at, and move with, the GBs. The second condition which should be met for full densification is rapid annihilation of the pores, as vacancies, at their adjacent GBs, despite the grain growth. The volume of the pores should be accommodated by diffusion at the available free volume of the GBs. Since these pores provide vacancies to the GB, they increase the chemical potential gradient at the GBs. Therefore some grain growth is inevitable at the final-stage sintering, which leads to a decrease in the GB free volume (GBFV). Nevertheless, densification with negligible grain growth may proceed if the sintering temperature is low enough to dominate the diffusion along the grain boundaries, yet suppress lattice diffusion within the grains.

In a well-equilibrated state in metals a GB may contain between 10% and 20% of free volume [39–44]. However, at the nanoscale size range, the GBFV significantly increases with the decrease in the grain size. Theoretical estimations [39,43,44] and experimental observations by various techniques [39–42] show that the free volume

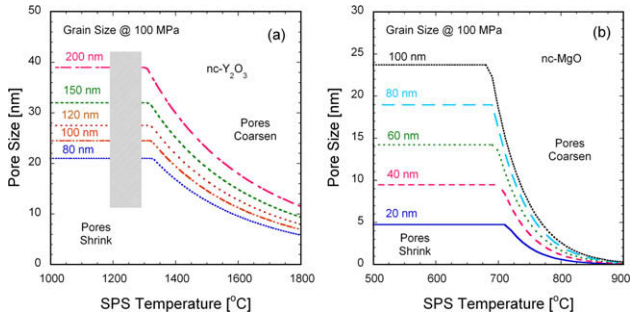

Figure 1. Pore size–grain size–SPS temperature densification maps for (a) nc-Y_2O_3 and (b) nc-MgO, at the final-stage sintering. The most appropriate SPS temperatures for full densification with rapid kinetics are at the right side of the plateaux (i.e. hatched region in (a)).

may comprise up to 44% of the GB volume in nc metals. Therefore, the GBFV difference between the nanoscale and the conventional size grains is higher than 10%, which is sufficient for the absorption of the pore volume during final-stage sintering.

Let us assume that at the start of final-stage sintering the relative density is 0.92. The pore volume per grain volume at this stage is 0.08, and all the pores are located at the grain corners. Densification to full density, to achieve optical transparency, will proceed as long as the pores are kept at the grain corners at different grain sizes; this dictates a critical relation between the grain size and the pore size.

The total pore volume per grain volume is given by:

$$V_p = N_v V_p^0, \tag{4}$$

where N_v is the number of pores per grain volume and V_p^0 is the volume of a single pore. N_v for TKDH grain is given by [32]:

$$N_V = \frac{6}{V_{TKDH}}, \tag{5}$$

where V_{TKDH} is the grain volume.

Using Eqs. (4) and (5), and substituting the appropriate expressions for the volumes of the TKDH grain ($V_{TKDH} = \frac{8\sqrt{2}}{27} G^3$) [45] and tetrahedral (Reuleaux) pore ($V_p^0 \approx 0.422 r^3$) [46], results in:

$$V_p = 6.04 \frac{r^3}{G^3}. \tag{6}$$

Therefore, the second condition for densification to full density may be set by equating the total pore volume per grain volume to 0.08:

$$r < 0.236 \cdot G. \tag{7}$$

Hence, one should seek the highest SPS temperature for which the pore size satisfies both conditions, i.e. Eqs. (3) and (7). These conditions were plotted in Figure 1 in terms of pore size–grain size–temperature assuming $\rho_{GB}/\rho_g = 0.80$ [44], $\rho = 0.92$, $\phi = 2\pi/3$, $\delta_{GB} = 10^{-9}$ [m] and $P_a = 100$ [MPa]. The data used to plot the curves in Figure 1 for nc-Y_2O_3 and nc-MgO are listed below. The following data were used for Y_2O_3: $D_s = 2.41 \times 10^{-8}$ [$m^3\ s^{-1}$] exp(−184 [kJ mol^{-1}]/RT) [47], $D_{gb} = 1.65 \times 10^{-6}$ [$m^2\ s^{-1}$] exp(−290 [kJ mol^{-1}]/RT) determined from the sintering tests [48], $\delta_s = 2 \times 10^{-9}$ [m], $\gamma_{sv} = 1.66$ [J m^{-2}] [49]. The following data were used for MgO: $D_s\delta_s = 3.80 \times 10^{-20}$ [$m^3\ s^{-1}$] exp(−161 [kJ mol^{-1}]/RT) [50], $D_{gb}\delta_{GB} = 3.45 \times 10^{-9}$ [$m^2\ s^{-1}$] exp(−402 [kJ mol^{-1}]/RT) [51], and $\gamma_{sv} = 1.1$ [J m^{-2}] [52].

Based on the two densification conditions, the curves in Figure 1 present the pore size at a given grain size and temperature, below which full densification may take place by diffusional processes and nanopore drag. Therefore, the temperature range (i.e. $\Delta T = 100$ °C) in which fast GB diffusion kinetics is associated with low risk for pore coarsening is located on the right side of the plateau of each curve (i.e. the hatched area in Fig. 1a). In this respect, the appropriate temperature for full densification of nc-Y_2O_3 at final-stage sintering with average grain size below 200 nm is ~1250 °C. The temperature range at which the curves convert to plateaux is important and may be used as a guide for the maximal densification temperature. The experimentally observed temperature of 1400 °C for the same nc-Y_2O_3 powder, above which pores were detached from the GBs [53], is in good agreement with the present calculated temperatures.

The financial support of the Israel Ministry of Science under Contract # 3-3429 is gratefully acknowledged. We thank Prof. Eugene Rabkin from Technion for his critical review of this paper.

[1] T. Ikegami, T. Mori, Y. Yajima, S. Takenouchi, T. Misawa, Y. Moriyoshi, J. Ceram. Soc. Japan 107 (1999) 297.
[2] L. Wen, X. Sun, Q. Lu, G. Xu, X. Hu, Opt. Mater. 29 (2006) 239.
[3] K. Tsukuma, J. Ceram. Soc. Jpn. 114 (2006) 802.
[4] G. Bernard-Granger, C. Guizard, L. San-Miguel, J. Am. Ceram. Soc. 90 (2007) 2698.
[5] S.N. Bagayev, V.V. Osipov, M.G. Ivanov, V.I. Solomonov, V.V. Platonov, A.N. Orlov, A.V. Rasuleva, S.M. Vatnik, Opt. Mater. 31 (2009) 740.
[6] J. Mouzon, A. Maitre, L. Frisk, N. Lehto, M. Oden, J. Eur. Ceram. Soc. 29 (2009) 311.
[7] B.N. Kim, K. Hiraga, K. Morita, H. Yoshida, Scripta Mater. 57 (2007) 607.
[8] B.N. Kim, K. Hiraga, K. Morita, H. Yoshida, J. Eur. Ceram. Soc. 29 (2009) 323.
[9] M. Suarez, A. Fernandez, J.L. Menendez, R. Torrecillas, Scripta Mater. 61 (2009) 931.
[10] Y. Aman, V. Garnier, E. Djurado, J. Eur. Ceram. Soc. 29 (2009) 3363.
[11] D.T. Jiang, D.M. Hilbert, U. Anselmi-Tamburini, T. Ng, D. Land, A.K. Mukherjee, J. Am. Ceram. Soc. 91 (2008) 151.
[12] R. Chaim, Z. Shen, M. Nygren, J. Mater. Res. 19 (2004) 2527.
[13] N. Frage, S. Cohen, S. Meir, S. Kalabukhov, M.P. Dariel, J. Mater. Sci. 42 (2007) 3272.
[14] C. Wang, Z. Zhao, Scripta Mater. 61 (2009) 193.
[15] S. Meir, S. Kalabukhov, N. Froumin, M.P. Dariel, N. Frage, J. Am. Ceram. Soc. 92 (2009) 358.
[16] K. Morita, B.N. Kim, K. Hiraga, H. Yoshida, Scripta Mater. 58 (2008) 1114.
[17] G. Bernard-Granger, N. Benameur, C. Guizard, M. Nygren, Scripta Mater. 60 (2009) 164.

[18] G. Zhang, Y. Wang, Z. Fu, H. Wang, W. Wang, J. Zhang, S.W. Lee, K. Niihara, J. Eur. Ceram. Soc. 29 (2009) 2705.
[19] R. Chaim, M. Kalina, J.Z. Shen, J. Eur. Ceram. Soc. 27 (2007) 3331.
[20] H. Mingsheng, L. Jianbao, L. Hong, G. Gangfeng, L. Long, J. Rare Earths 24 (2006) 222.
[21] U. Anselmi-Tamburini, J.N. Woolman, Z.A. Munir, Adv. Func. Mater. 17 (2007) 3267.
[22] J.E. Alaniz, F.G. Perez-Gutierrez, G. Aguilar, J.E. Garay, Opt. Mater. 32 (2009) 62.
[23] J.G.J. Peelen, R. Metselaar, J. Appl. Phys. 45 (1974) 216.
[24] R. Apetz, M.P.B. van Bruggen, J. Am. Ceram. Soc. 86 (2003) 480.
[25] A. Krell, J. Klimke, T. Hutzler, Opt. Mater. 31 (2009) 1144.
[26] R. Chaim, O. Reinharz Bar-Hama, Mater. Sci. Eng. A 527 (2010) 462.
[27] K.J. Yoon, S.-J.L. Kang, J. Eur. Ceram. Soc. 6 (1990) 201.
[28] A.V. Sergueeva, N.A. Mara, N.A. Krasilnikov, R.Z. Valiev, A.K. Mukherjee, Phil. Mag. 86 (2006) 5797.
[29] M. Sakai, H. Muto, Scripta Mater. 38 (1998) 909.
[30] H. Muto, Y. Takahashi, T. Futami, M. Sakai, J. Eur. Ceram. Soc. 22 (2002) 2437.
[31] R. Chaim, R. Marder-Jaeckel, J.Z. Shen, Mater. Sci. Eng. A (2006) 74.
[32] R. Marder, R. Chaim, C. Estournes, Mater. Sci. Eng. A 527 (2010) 1577.
[33] I.W. Chen, X.H. Wang, Nature 404 (2000) 168.
[34] R. Dannenberg, E. Stach, J.R. Groza, J. Mater. Res. 16 (2001) 1090.
[35] R.J. Brook, J. Am. Ceram. Soc. 52 (1969) 56.
[36] C.A. Handwerker, R.M. Cannon, R.L. Coble, in: W.D. Kingery (Ed.), Advances in Ceramics, vol. 10, American Ceramic Society, Columbus, OH, 1984, pp. 619–643.
[37] C.H. Hsueh, A.G. Evans, R.L. Coble, Acta Metall. 30 (1982) 1269.
[38] S.-J.L. Kang, Y.-I. Jung, Acta Mater. 52 (2004) 4573.
[39] M. Wagner, Phys. Rev. B 45 (1992) 635.
[40] P.P. Chatterjee, S.K. Pabi, I. Manna, J. Appl. Phys. 86 (1999) 5912.
[41] Y. Zhou, S. Van Petegem, D. Segers, U. Erb, K.T. Aust, G. Palumbo, Mater. Sci. Eng. A 512 (2009) 39.
[42] W. Xu, X. Song, N. Lu, C. Huang, Acta Mater. 58 (2010) 396.
[43] P.P. Chattopadhyay, S.K. Pabi, I. Manna, Mater. Chem. Phys. 68 (2001) 80.
[44] X. Song, J. Zhang, L. Li, K. Yang, G. Liu, Acta Mater. 54 (2006) 5541.
[45] J.E. Hilliard, in: H. Elias (Ed.), Streology, Springer, Berlin, 1967, p. p. 211.
[46] E.W. Weisstein, Reuleaux Tetrahedron, MatWorld – A Wolfram Web Resource. Available from: <http://mathworld.wolfram.com/ReuleauxTetrahedron.html>.
[47] M.F. Berard, D.R. Wilder, J. Appl. Phys. 34 (1963) 2318.
[48] M.F. Berard, D.R. Wilder, J. Am. Ceram. Soc. 52 (1969) 85.
[49] P. Zhang, A. Navrotsky, B. Guo, I. Kennedy, A.N. Clark, C. Lesher, Q. Liu, J. Phys. Chem. C112 (2008) 932.
[50] S. Kleiman, R. Chaim, Mater. Lett. 61 (2007) 4489.
[51] R. Chaim, M. Margulis, Mater. Sci. Eng. A 407 (2005) 180.
[52] J.J. Gilman, J. Appl. Phys. 31 (1960) 2208.
[53] R. Chaim, A. Shlayer, C. Estournes, J. Eur. Ceram. Soc. 29 (2009) 91.